Research Square

Preprints are preliminary reports that have not undergone peer review.
They should not be considered conclusive, used to inform clinical practice,
or referenced by the media as validated information.

Pharmacological enhancement of 20S proteasome-mediated degradation exposes a vulnerability in human papillomavirus (HPV)-driven cervical cancer

Jetze Tepe

cew9xb@virginia.edu

University of Virginia https://orcid.org/0000-0001-5467-5589

Shannon Cartwright

University of Virginia https://orcid.org/0009-0009-5946-6351

Linh Le

University of Virginia

Allison Carranza

University of Virginia

Kate Hartnett

University of Virginia

Bahareh Ghaffari

Michigan State University

Yue Dou

University of Virginia https://orcid.org/0009-0003-5557-0852

Guruprasad Konduru

University of Virginia

Pankaj Kumar

University of Virginia https://orcid.org/0000-0002-8702-8879

Tian Zhang

University of Virginia

Article

Keywords:

Posted Date: November 9th, 2026

DOI: https://doi.org/10.21203/rs.3.rs-11244820/v1

License: This work is licensed under a Creative Commons Attribution 4.0 International License.
Read Full License

Additional Declarations: (Not answered)

Pharmacological enhancement of 20S proteasome-mediated degradation exposes a vulnerability in human papillomavirus (HPV)-driven cervical cancer

Shannon M. Cartwright[a], Linh T. Le[a], Allison Carranza[a], Kate A. Hartnett[a], Bahar Ghaffari[b], Yue Dou[c], Guruprasad Konduru[d], Pankaj Kumar[d], Tian Zhang[c], Jetze J. Tepe[a,*]

[a]*Department of Chemistry, University of Virginia, Charlottesville VA, USA*

[b]*Department of Chemistry, Michigan State University, East Lansing MI, USA*

[c]*Department of Biochemistry and Molecular Genetics, University of Virginia, Charlottesville VA, USA*

[d]*Bioinformatics Core, University of Virginia, Charlottesville VA, USA*

[*]*Corresponding Author email: cew9xb@virginia.edu*

Abstract: Despite the availability of prophylactic vaccines against human papillomavirus (HPV), infection and subsequent cervical cancer remain a significant global health problem. HPV viral oncoproteins E6 and E7 drive oncogenesis, in part through disruption of cell growth control pathways via degradation of the tumor suppressors p53 and pRB, respectively. These proteins contain intrinsically disordered regions that enable interactions with multiple cellular targets but also complicate the development of conventional therapeutics. While these proteins have previously been associated with a ubiquitin-dependent clearance mechanism through the 26S proteasome, we show that these HPV viral proteins can be degraded in a ubiquitin-independent method through the 20S proteasome alone. We also show that the small molecule-enhancement of this protease reduces HPV E6 and E7 protein levels across high-risk strains of the virus in a proteasome-dependent and transcription-independent manner. 20S proteasome activation suppressed HPV-driven phenotypes, including reduced proliferation and restoration of cell-cycle regulatory signaling. Whole cell proteomic analysis revealed remodeling of cancer-

23 associated pathways including shifts consistent with reduced proliferative and oncogenic
24 metabolic signaling. Collectively, these findings identify a previously unrecognized vulnerability
25 of HPV oncoproteins and establish 20S proteasome activation as a potential therapeutic strategy
26 for HPV-associated cancers.

Introduction

Human papillomaviruses (HPVs) are among the most common sexually transmitted infections, and high-risk (HR) HPVs are responsible for approximately 5% of cancers globally, most notably cervical cancer.[1-4] Despite the presence of prophylactic vaccines, inoculation levels remain low,[5] and there is no cure for established HPV infection.[2]

Following HR HPV infection, the host cell begins producing viral proteins, including HPV oncoproteins E6 and E7.[2, 4] These proteins have heightened disordered structures which enable their interactions with many different targets, allowing their manipulation of a wide range of protein networks.[4, 6-8] Most notably, E6 and E7 induce the degradation of tumor suppressor proteins p53 and pRB, respectively.[2-4] This allows infected cells to resist cell death and proliferate uncontrollably, leading to genomic instability and the development of cancer.[3, 4] Once malignant transformation has occurred, HR HPV E6 and E7 remain essential for tumor maintenance and progression, in part by promoting metabolic reprogramming to favor glycolysis over oxidative phosphorylation[9-15] and facilitating cancer metastasis through the epithelial-mesenchymal transition (EMT).[16-22]

Proteins with intrinsically disordered structures (IDPs) are challenging to target using small molecules due to their lack of well-defined binding pockets.[6, 23, 24] The primary protease responsible for the degradation of IDPs in cells is the 20S proteasome. The 20S proteasome can associate with the 19S cap to form the 26S proteasome, and the two forms coexist in equilibria.[25] In most cells, including HPV18+ HeLa cells, the 20S is the dominant form.[25-27] Unlike the 26S proteasome, the 20S can directly recognize IDPs without ubiquitinylation.[28-31] While HPV E6 and E7 are known to have disordered termini,[6, 8, 32] their susceptibility to ubiquitin-independent degradation has not been established.

Here, we demonstrate that maintenance of cellular HPV E6 and E7 protein levels does not require 26S-mediated degradation and that pharmacological activation of the 20S proteasome enhances degradation of these viral IDPs. This provides the first evidence that HR HPV E6 and E7 can be targeted through 20S proteasome–mediated degradation and establishes a new strategy to therapeutically combat these proteins. We assessed the impact of pharmacologic activation of the 20S proteasome using two structurally unrelated small-molecule 20S enhancers, TCH-165,[25, 33-35] and a newly identified compound, MM. Both enhancers showed consistent reductions of HPV oncoproteins across HR HPV types in proteasome-dependent and transcription-independent manners. Consistent with the dependence upon HR E6 and E7 for cancer progression, proteasome enhancement was associated with decreased cellular proliferation, altered cell cycle progression, and broad remodeling of HPV cancer-associated pathways. Whole cell proteomics and pathway enrichment analysis showed that both compounds altered pathways associated with tumor progression, including increased representation of proteins involved in oxidative phosphorylation and decreased representation of proteins in metastasis and proliferation pathways. Collectively, this work links the 20S proteasome to the degradation of viral oncoproteins E6 and E7 and supports pharmacological 20S proteasome enhancement as a potential strategy to disrupt HPV-driven tumor biology.

Results

The 20S proteasome can degrade HPV18 E7 in-vitro

Due to the understudied nature of the 20S proteasome, it has often been overlooked when identifying protein degradation mechanisms. Since the disordered termini on HR HPV E6 and E7 suggests they could be targets for 20S proteasome-mediated degradation, we first investigated if the 20S proteasome alone could degrade HPV18 E7 in a purified enzyme assay. After three hours

of incubation, the proteasome containing samples had 55.3 ± 7.02% (p=0.0066) of HPV18 E7 compared to samples without any 20S proteasome (Fig. 1A). It is important to note that it has been widely shown that in purified systems HR E7 proteins are primarily in a dimerized form,[8, 36] suggesting that its degradation is influenced by both the population of protein in the monomeric form and the activity of the proteasome toward the substrate. Regardless, this experiment is the first to demonstrate that the 20S proteasome can degrade HPV18 E7 protein in a ubiquitin-independent manner.

Cellular inhibition of the 20S proteasome impacts HPV18 E7 protein levels whereas 26S proteasome and autophagy inhibition do not

To understand if the 20S proteasome is involved in degrading E6 and E7 in cells where alternative degradation pathways are also present, we inhibited the main protein degradation pathways and measured the effect on HPV oncoprotein levels. First, Bafilomycin A1 (BAF), a known autophagy inhibitor,[37] was used. Autophagy inhibition in HPV18+ HeLa cells had no impact on E6 and E7 levels (E6: 64.8 ± 19.2%, p=0.8655; E7: 104.0 ± 42.6%, p=0.9948) (Fig. 1B).

The other common proteolysis pathway is through the proteasome. Previous studies have demonstrated that inhibition with Bortezomib (BTZ) resulted in an accumulation of E6 and E7.[38, 39] Bortezomib inhibits the catalytic sites of the 20S core particle, and therefore inhibits both the 20S and 26S proteasomes indistinguishably.[40] In the presence of bortezomib, we saw similar E6 and E7 accumulation in HPV18+ cells as demonstrated in literature,[38] confirming some form of functioning proteasome was necessary for both proteins' baseline clearance (Fig. 1C).

Next, we sought to determine which proteasome species is required for cellular HPV oncoprotein degradation. Selective inhibition of the 26S proteasome-mediated degradation pathway was conducted in three different ways, either through inhibiting the de-ubiquitination or unfolding abilities of the 19S cap or through the inhibition of 26S assembly. The PSMD14 subunit of the 19S cap was inhibited using small-molecule Capzimin (treatment A).[41] This subunit is the de-ubiquitinase in the 19S cap that allows for ubiquitin-tagged proteins to be moved into the catalytic core for degradation.[41, 42] Alternatively, siRNA for PSMC5, an ATPase required for 26S proteasome activity,[43, 44] or PSMD11, a non-ATPase subunit involved in 26S assembly,[45, 46] were individually used to knockdown the 26S proteasome-mediated protein degradation (treatments B and C, respectively). K48 polyubiquitinylation levels were used to measure effectiveness of the treatment (Fig. 1C), along with western blotting for the subunits in the cases where siRNA was used (Fig. S1). While K48 polyubiquitinylated proteins accumulated (Fig. 1C), demonstrating successful ubiquitin-dependent 26S proteasome inhibition, HPV18 E6 and E7 protein levels were unchanged (E6 Treatment B: 144.3 ± 49.8%, p=0.7427; Treatment C: 105.3 ± 38%, p=0.9997; E7 Treatment A: 55.5 ± 24.5%, p=0.1242; Treatment B: 72.0 ± 16.5%, p=0.5934; Treatment C: 75.0 ± 8.9%, p=0.4524) or even decreased in some instances (E6 Treatment A: 37.8 ± 13.5%, p=0.0019) (Fig. 1C). Although E6 and E7 have previously been associated with ubiquitin-dependent degradation pathways,[47] the lack of protein accumulation upon inhibition of the 26S proteasome supports our hypothesis that these proteins can be degraded by the 20S proteasome alone.

In-vitro identification of 20S proteasome enhancers

With our new understanding of the protein degradation machinery involved in HPV oncoprotein clearance, we wanted to see if pharmacological enhancement of the 20S proteasome

could be used to increase the removal of the viral proteins. TCH-165 (Fig. 2A) was previously identified as a 20S proteasome enhancer.[25] Another, structurally distinct, compound, MM (Fig. 2A), was identified from an internal library high-throughput screening campaign[48] and is reported as a proteasome enhancer for the first time here. Small-molecule impact on 20S proteasome-mediated degradation was measured using a kinetic fluorogenic small peptide-based assay (Fig. 2B). The rate of fluorescence is proportional to the proteolytic activity, with the concentration where 200% increase in the rate of proteolysis relative to vehicle is defined as the EC_{200}. Both compounds demonstrated comparable activities, with EC_{200} values of 1.48 ± 0.37 μM (TCH-165) and 1.43 ± 0.72 μM (MM) (Fig. 2B). Maximal activity at the highest concentration tested is also reported (Fig. 2B).

Identified compounds do not impact the 26S proteasome

Prior studies have shown that TCH-165 specifically enhances the activity of the 20S proteasome over the 26S,[25] confirmed here (Fig. 2B). To determine whether MM exhibits similar selectivity, we adapted the fluorogenic substrate assay to directly measure 26S proteasome activity. In contrast to its robust enhancement of 20S proteasome activity, MM did not enhance 26S proteasome-mediated proteolysis (Fig. 2B).

Proteasome enhancers reduce cellular HPV16/18 oncoprotein levels

We hypothesized that proteasome enhancement could be used to reduce HPV oncoproteins. To test this, HPV18+ cells (HeLa) were treated with each proteasome enhancer individually, at both 5 and 10 μM concentrations for 24 hours. Both compounds reduced HPV18 E6 and E7 protein levels in a dose-dependent manner (Fig. 2C). 10 μM of TCH-165 and MM

significantly decreased both E7 levels (49.6 ± 25.5%, p=0.0348; 37.4 ± 14.2%, p=0.0096, respectively) and E6 levels (42.4 ± 19.5%, p=0.0260, 31.4 ± 22.8%, p=0.0012, respectively).

Next, we assessed the two compounds' effects in another HR HPV strain. HPV16+ cells (CaSki) were treated with each compound at 1, 2.5, 5, and 10 μM for 24 hours. Due to limitations in antibody performance, HPV16 E7 levels were measured by ELISA, and HPV16 E6 was not evaluated. Both compounds reduced HPV16 E7 levels in a dose-dependent manner, with near complete reduction observed at 10 μM (TCH-165: 4.33 ± 0.577%, p<0.0001; MM: 1.67 ± 0.577%, p<0.0001) (Fig. 2D).

Compound impact is dependent upon a functioning proteasome and is transcription independent

To validate that the mechanism of action for the compounds' impacts on HPV oncoproteins was through the proteasome, we performed pre-treatments with proteasome inhibitor Bortezomib prior to dosing with 20S proteasome enhancers. With the proteasome inhibitor present, the compound-induced reduction in HPV18 E6 and E7 levels was abolished (Fig. 2E), indicating that their observed effects were dependent on proteasome function.

Next, we confirmed that HPV protein level changes did not occur due to decreased HPV18 *E6E7* transcription using RT-qPCR. Neither compound significantly affected RNA abundance (Fig. 2F) (TCH-165 p=0.7137; MM p=0.9837), indicating that the observed effects arise from post-transcriptional regulation, consistent with increased proteasomal degradation.

Proteasome enhancement impact on downstream p53 and pRB pathways

Due to the relationship between E6 and p53, we wanted to see if the proteasome-enhanced degradation of the viral protein would impact p53 levels. A p53 ELISA was used to measure protein levels in HPV16+ cellular samples treated with both proteasome enhancers (Fig.

3A). Only MM enhanced p53 levels significantly (211.3 ± 13.61%, $p<0.0001$). In HPV18+ cells, the same experiment was attempted, however, no significant change was seen in p53 levels at the 24-hour treatment timepoint (Fig. S2).

RT-qPCR was used to assess the expression of genes downstream of p53 and pRB in HPV+ cells (Fig. 3B). *CDKN1A* (encoding p21) is transcriptionally controlled by p53 and activates pRB.[49] *TK1* is transcriptionally activated by E2F, which gets inhibited by pRB.[50, 51] Interestingly, *CDKN1A* was significantly upregulated following treatment in HPV18+ cells (TCH-165: $Log_2(FC)=1.92 \pm 0.327$, $p=0.0057$; MM: $Log_2(FC)=1.54 \pm 0.464$, $p=0.0171$). *TK1* expression showed a downward trend that did not reach statistical significance (Fig. 3B). In HPV16+ cells, similar results were seen with a significant increase in *CDKN1A* (TCH-165: $Log_2(FC)=0.996 \pm 0.127$, $p=0.0026$; MM: $Log_2(FC)=1.27 \pm 0.099$, $p=0.0007$) and a downward but non-significant trend in *TK1*. These results are consistent with modulation of cell cycle regulatory pathways downstream of p53 and pRB.[49-52]

20S proteasome enhancement inhibits HPV+ cervical cancer growth

We next investigated the functional consequences of enhanced 20S proteasome-mediated oncoprotein degradation. Cell viability assays were performed on HPV+ cells dosed for 72 hours with varying concentrations of either proteasome enhancer, utilizing an ATP measurement assay to compare viability levels in treated samples to the untreated vehicle (Fig. 3C). Both compounds had an impact on cell viability: in HPV18+ cells, the compounds had IC_{50} values of 8.2 ± 0.9 μM (TCH-165) and 7.3 ± 1.2 μM (MM), and in HPV16+ cells, they had IC_{50} values of 5.4 ± 0.4 μM (TCH-165) and 8.3 ± 0.8 μM (MM). To distinguish between cytotoxic and anti-proliferative effects, a multiplexed toxicity assay was performed (Fig. 3C). Both compounds exhibited low toxicity at concentrations ≤10 μM despite substantial reductions in ATP levels (~50%) in the

same samples, suggesting that the observed reduction in viability is driven predominantly by halting cellular proliferation rather than cell death.

To determine treatment impact on sustained proliferative capacity and colony formation, we performed clonogenic assays. Cells were treated for 24 hours before removing compound and allowing the culture to grow for an additional 14 (HPV18+) or 22 days (HPV16+). These studies showed that compound treatment resulted in less dense colony formation than the untreated control (Fig. 3D, Fig. S3). This demonstrates that proteasome enhancement can reduce long-term proliferative capacity in HPV+ cells.

Based on our hypothesis that proteasome enhancement slowed cell growth through an impact on the cell cycle, we measured HPV+ cell cycle distribution using flow cytometry (Fig. 3E-F). Treatment with either compound resulted in fewer cells in the G2/M phase compared to the untreated vehicle in both HR HPV cell lines (HPV18+ Vehicle: 11.32 ± 1.30; TCH-165: 7.71 ± 1.07, p=0.0201; MM: 7.52 ± 1.89, p=0.0156. HPV16+ Vehicle: 12.10 ± 3.66; TCH-165: 1.26 ± 0.30, p=0.0003; MM: 4.27 ± 1.15, p=0.0028) (Fig. 3E-F). In HPV18+ cells, TCH-165 also significantly increased the percentage of the cells in the G0/1 phase (Vehicle: 59.50 ± 3.32; TCH-165: 69.32 ± 1.64, p= 0.0012). In HPV16+ cells, MM had this effect (Vehicle: 63.18 ± 9.05; MM: 83.79 ± 3.15, p=0.0023) (Fig. 3F) along with a significant reduction of cells in the S phase (Vehicle: 24.72 ± 5.41; MM: 11.94 ± 2.18, p=0.0027) (Fig. 3F). Together, this data suggests that proteasome enhancer-mediated degradation of HPV oncoproteins promotes tighter cell-cycle regulation in HR HPV+ cells.

Proteasome enhancement has a diverse impact on the HPV18+ cervical cancer proteome

To assess the effects of proteasome enhancement on the global cellular proteome, we analyzed HPV18+ cells by quantitative proteomics after 24 hours of treatment with proteasome enhancers. Whole-cell mass spectrometry-based analysis identified around 6600 proteins per sample (Fig. 4A) and allowed us to quantify differential protein abundance relative to vehicle controls (Fig. 4B). DEqMS[53] R package was used to perform the differential protein analysis. Gene set enrichment analysis done using fgsea and pathway reference databases from the Molecular Signatures Database (MSigDB)[54] hallmark gene sets revealed decreased E2F targets and G2/M checkpoint signaling, along with increased oxidative phosphorylation signatures (Fig. 4C-D). Additional pathway changes included reduced epithelial-mesenchymal transition (EMT)-associated signaling (MM) and increased apoptosis-associated pathways (TCH-165). This data indicates that 20S proteasome enhancement broadly remodels cancer-associated pathways.

Discussion

Despite their appeal as a therapeutic target, HPV viral oncoproteins remain a challenge to regulate pharmacologically due to their disordered nature. The 20S proteasome is the preferred protease for the degradation of IDPs. Enhancement of 20S proteasome-mediated proteolysis therefore provides a novel strategy for targeting these oncoproteins. This work establishes that HPV viral oncoproteins can be targeted for degradation by the 20S proteasome both in purified (Fig. 1A) and cellular systems (Fig. 1B-C). Cellularly, inhibition of the main proteolysis pathways was used to understand the role each played in maintaining HPV viral protein levels. Through three different mechanisms, we inhibited 26S proteasome-mediated protein degradation, but we did not see any subsequent buildup of HPV18 E6 or E7 protein levels (Fig. 1C). These findings suggest that HPV viral proteostasis does not require ubiquitin-dependent 26S proteasome-mediated degradation and supports a role for 20S-mediated turnover of these

oncoproteins. While inhibition of autophagy also did not prevent HPV18 E6 and E7 protein degradation (Fig. 1B), global proteasome inhibition did (Fig. 1C). After implicating the 20S proteasome as a novel degradation mechanism for HPV viral proteins, we determined whether we could target 20S-mediated proteolysis to further reduce E6 and E7 protein levels and impact HPV-mediated cancer phenotypes.

We identified a novel 20S proteasome enhancer (MM, Fig. 2A) and demonstrated its selectivity for the 20S over the 26S proteasome (Fig. 2B). We utilized this compound, along with a previously published 20S proteasome enhancer, TCH-165 (Fig. 2A), to demonstrate the efficacy of 20S proteasome-mediated degradation of E6 and E7 across HR HPV strains (Fig. 2C-D). Mechanistic studies confirmed that the compound activity is dependent on a functional proteasome, as demonstrated through the abrogation of their activity in the presence of a proteasome inhibitor (Fig. 2E). RT-qPCR confirmed that the compounds do not impact oncoprotein synthesis (Fig. 2F).

E6 and E7 proteins result in the constant removal of p53 and pRB, two cell cycle checkpoints controlling cell growth.[1, 3, 4, 55, 56] When studying the impact proteasome-enhancement had on p53, only MM treatment in HPV16+ cells resulted in a significant increase in p53 levels (Fig. 3A). HPV18+ cells saw no change in p53 levels at the timepoint studied (Fig. 2S). However, this is consistent with literature reports that show rises in p53 levels are transient even under consistent E6 knockdown in HeLa cells, likely due to tight regulation.[52, 57, 58]

RT-qPCR gave further support that proteasome enhancement was influencing downstream tumor suppressor pathways. *CDKN1A* encodes for p21, a protein whose levels are activated by p53 and inhibits the E2F pathway through pRB activation.[49] RT-qPCR studies

revealed that compound treatment increased *CDKN1A* RNA levels in both HPV+ cell lines (Fig. 3B), consistent with p53 control being restored.

p53 controls cell cycle arrest and can induce apoptosis if the cell experiences too much stress.[3] pRB controls the transcription of genes needed for the S phase of cell cycle by inhibiting transcription factor E2F.[3, 59] HPV induced dysregulation of these pathways allows cells to move uncontrolled through their cell cycle.[59] Consistent with a reduction in E6 and E7 levels, proteasome enhancement impacted cellular proliferation and cell cycle distribution in both HPV+ cell lines (Fig. 3C-F). Both proteasome enhancers had a dose-dependent reduction in viable cells (Fig. 3C) in both HPV18+ and HPV16+ cells, with higher concentrations (≥5 μM) reducing ATP levels in culture substantially. However, when measuring cell death directly, the compounds did not show toxicity levels which could account for this reduced viability. We hypothesize that proteasome enhancement has an anti-proliferative effect on the cells due to the reduction of E6 and E7, since slowed cell growth is a downstream consequence of HPV oncoprotein suppression.[60, 61] Clonogenic assays demonstrated that 20S proteasome enhancement can have long-term impacts on cellular growth weeks after treatment (Fig. 3D). When looking at cell cycle distribution, we saw that proteasome enhancement significantly decreases the number of cells in the G2/M phase in both HR HPV strains (Fig. 3D-F). Significant increases in the number of cells in the G0/G1 phases were also seen, differing between cell type which compound caused it (HPV18+ cells – TCH-165; HPV16+ cells – MM) (Fig. 3F).

Whole cell global proteomics experiments were done on HPV18+ cells to understand what impact this strategy has overall (Fig. 4A-D). Gene set enrichment analysis showed that the pathways affected by compound treatment are consistent with degradation of HPV oncoproteins, restoration of p53 and pRB function, and controlled cell cycle regulation (Fig. 4C). Pathway

analysis performed using differentially expressed protein expression shows proteasomal enhancement inhibits E2F targets, including TK1,[50, 51] consistent with restoration of pRB-regulated signaling (Fig. 4D). A decrease in G2/M checkpoints was also seen, supporting the cell cycle experimental results where cells are getting stalled before they can exit at mitosis.

E6 and E7 also play roles supporting cancer survival through metabolic reprogramming and metastasis.[9-14] These oncoproteins remove inhibitors to glycolysis and repress oxidative phosphorylation while simultaneously upregulating sterol regulatory element-binding proteins (SREBPs) to promote lipid and sterol synthesis.[9-14, 62-66] Proteasome enhancement, however, increased proteins in the oxidative phosphorylation pathway (Fig. 4C) with MM treatment specifically lowering proteins in the cholesterol homeostasis pathway (Fig. 4C), SREBPs (Fig. 4D), supporting a shift away from HPV altered metabolism. In parallel, E6 and E7 promote cancer metastasis and invasion through the activation of signaling pathways like Wnt/β-catenin, allowing cells to gain an invasive ability through the disruption of their cell adhesion properties by an epithelial-mesenchymal transition (EMT).[16-21] Proteomics pathway analysis shows that proteasome enhancement decreases wnt/β-catenin pathway proteins (Fig. 4C-D). MM treatment also showed an activation of the adipogenesis cell differentiation pathway, which opposes EMT,[67] and a downregulation of the EMT pathway itself (Fig 4C). This data suggests that proteasome enhancement can result in a general rewiring of pathways manipulated by HPV-mediated cancers to survive and spread.

Altogether, we have established a novel protein degradation mechanism for HPV viral proteins through the 20S proteasome and showed that enhancement of that pathway can be utilized to deplete E6 and E7 levels in two of the highest risk viral strains. We selectively enhanced 20S-mediated proteolytic activity with two structurally diverse small molecules,

reducing HR HPV E6 and E7 levels in cells. Mechanistic studies supported that compound impact on the oncoproteins is through proteasomal degradation. We also showed downstream effects of this oncoprotein reduction, with proteasome enhancement slowing cell growth through stalling of the cell cycle. Finally, whole cell proteomics showed that both proteasome enhancers had a wide-reaching effect on many different pathways impacted by HPV and oncogenesis, inducing a shift away from conditions which favor cancer progression. Altogether, these findings identify a previously unrecognized vulnerability of HPV oncoproteins and establish 20S proteasome activation as a potential therapeutic strategy for HPV-associated cancers.

Materials and Methods

Cell culture

HeLa (HPV18+) (Cytion, Souix Falls, SD #300194) and CaSki (HPV16+) (ATCC, Manassaas, VA #CRL-1550,) were cultured according to suppliers instructions. HeLa growth media: EMEM (ATCC# 30-2003) medium supplemented with 10% FBS (Gibco, Grand Island, NY #A5670701), 1% penicillin-streptomycin (Gibco #15140122) and 100 ug/mL Normocin (Invivogen, San Diego, CA #ant-nr-05). CaSki growth media: RPMI-1640 (ATCC #30-2001) medium supplemented with 10% FBS (Gibco #A5670701), 1% penicillin-streptomycin (Gibco # 15140122) and 100 ug/mL Normocin (Invivogen #ant-nr-05). All cells were incubated at 37 ˚C and 5% CO_2 and tested regularly for mycoplasma (Invivogen #rep-mys-10).

Immunoblotting

Samples were resolved on 4-20% tris-glycine gels (Bio-Rad, Hercules, CA #4561094) in 1x tris/glycine/SDS running buffer (Bio-Rad #1610772) and transferred to membrane (0.2 µm nitrocellulose for HPV E6/E7, 0.2 µm PVDF for K48 polyubiquitin) using either iBlot 3 semi-

dry transfer system (Thermofisher Scientific, Waltham, MA #IB31001, iBlot 3 stacks from Thermofisher Scientific #IB33002) at RT or wet transfer using Mini Trans-blot Electrophoretic Transfer Cell (Bio-Rad #1703930, membrane from Bio-Rad #1620097) in cold transfer buffer (19 mM Tris HCl, 192 mM glycine, 10% methanol) for 45 minutes at 4 ˚C. The membranes were blocked with 5% milk (Bio-Rad #1706404) in 1x TBST (Tris-buffered saline Tween 20, 20 mM Tris, 150 mM NaCl, 0.1% tween 20) at RT for 1 hour. The desired primary antibody was added in 2% milk, 1x TBST at 4 ˚C overnight (16-20 hours). The blots were washed with 1x TBST 3 x 5 minutes before being incubated with the corresponding secondary antibody was added in 2% milk, 1x TBST for 1 hour at RT. The blots were developed with ECL western reagent (Azure Biosystems, Dublin, CA #AC2103) and imaged using an Azure Biosystems 300Q imager. The blots were stripped using mild stripping buffer (200 mM glycine, 1% Tween 20, 3.5 mM SDS, pH = 2.2) for 30 minutes at RT before being washed 3 x 5 minutes with 1x TBST and probed for the internal loading control added in 2% milk, 1x TBST for 1 hour at RT. Images were quantified using Image Lab software (Bio-Rad). See table below for antibodies and concentrations used.

Target	Concentration	Source
HPV18 E6 (G-7)	1:100	Santa Cruz Biotechnology, Dallas, TX #sc-365089
HPV18 E7 (F-7)	1:200	Santa Cruz Biotechnology #sc-365035
Anti-Mouse IgG HRP-conjugated	1:1000	Cell Signaling, Danvers, MA #7076V

Anti-Rabbit IgG HRP-conjugated	1:1000	Biotechne, Minneapolis, MN #HAF008
GAPDH (6C5cc) HRP-conjugated	1:1250	Biotechne #NB600-502H
20S Proteasome β5 (A-10)	1:200	Santa Cruz Biotechnology # sc-393931
K48 polyubiquitin (D9D5) HRP-conjugated	1:1000	Cell Signaling #12805
PSMD11 (D1T1R)	1:1000	Cell Signaling #14303
PSMC5/TRIP1	1:1000	Cell Signaling #13392

In-vitro 20S proteasome HPV18 E7 protein digestion assay

The HPV18 E7 protein digestion assay with the 20S proteasome occurred in 25 µL reaction volumes of buffer (50 mM HEPES, 150 mM NaCl, 0.2 mM DTT, 0.01% Tween 20, 25 µM EDTA, pH=7.5) HPV18 E7 (Sino Biological, Philadelphia, PA #40966-V07E, final concentration 100 nM) and 20S proteasome (R&D systems, Minneapolis, MN #E-360, final concentration 10 nM), incubated in 37 ˚C water bath for 3 hours. HPV18 E7 protein was first diluted in buffer (125 nM) and incubated at 25 ˚C for 30 minutes. 20S proteasome was diluted in buffer (50 nM). After the protein incubation time, the protein (20 µL) and 20S proteasome (5 µL) stocks were added to each tube and mixed gently. A mix of 4x SDS loading buffer (Bio-Rad #1610747, 58.31 µL) and GAPDH (Novus, Chesterfield, MO #NBC1-18528, 3.5 µL) were used as the digestion stopping solution. For the 0-hour samples, this stop solution (8.83 µL) was

added immediately, the solution mixed, and boiled for 10 minutes. The incubation samples were added to a 37 ˚C water bath for 3 hours before the stop solution (8.83 µL) was added and the samples boiled. All boiled samples were brought to room temperature (RT) before being stored at 4 ˚C overnight before immunoblotting.

Inhibition of autophagy in HPV18+ cells

HeLa cells (500,000 cells) were plated in 6 well plate in growth media (2-3 mL) and incubated overnight at 37 ˚C, 5% CO_2. The media was swapped with fresh media containing Bafilomycin (500 nM, 0.05% DMSO, 2 mL/plate) and incubated again at 37 ˚C, 5% CO_2 for 1 hour. If co-treatment occurred compounds or DMSO (1 µL, 0.05% DMSO, indicated compound concentration) were added directly to the media and incubating for 24 hours at 37 ˚C, 5% CO_2. For lysis, the cells were scraped, diluted in PBS (Thermofisher Scientific #10010023, 8 mL) and spun down and the pellets washed with PBS (0.5 mL) before being resuspended in lysis buffer (PBS (8 mL) + EDTA free protease inhibitor (Millipore Sigma, Burlington, MA #11836170001, 1 tablet), 50-80 µL) and lysed using sonication. The sonicated samples were centrifuged (2000 xg, 20-30 minutes, 4 ˚C) before the supernatant was removed and stored at -80 ˚C. A Pierce protein analysis kit (Thermofisher Scientific #23225) was used to determine the concentration of total protein levels in each sample following the manufacturer's instructions. The samples were analyzed using immunoblotting.

Inhibition of proteasomes (Bortezomib)

HeLa cells (1,600,000 cells) were plated in 6 cm plate in growth media (3 mL) and incubated overnight at 37˚C, 5% CO_2. The media was swapped with fresh media containing Bortezomib (Med Chem Express, Monmouth Junction, NJ #HY-10227; 300 nM, 0.1% DMSO, 4

mL/plate) and incubated again for 24 hours at 37˚C, 5% CO_2. For lysis, the cells were scraped, diluted in PBS (Thermofisher Scientific #10010023, 6 mL) and spun down and the pellets washed with PBS (0.5 mL) before being resuspended in lysis buffer (PBS (8 mL) + EDTA free protease inhibitor (Millipore Sigma #11836170001, 1 tablet), 50-80 µL) and lysed using sonication. The sonicated samples were centrifuged (2000 xg, 20-30 minutes, 4 ˚C) before the supernatant was removed and stored at -80 ˚C. A Pierce protein analysis kit (Thermofisher Scientific #23225) was used to determine the concentration of total protein levels in each sample following the manufacturer's instructions. The samples were analyzed using immunoblotting.

Inhibition of 26S proteasome – Capzimin

HeLa cells (1,600,000 cells/plate) were plated in 6 cm plates in growth media (3 mL) and incubated overnight at 37 ˚C, 5% CO_2. The next day, media was removed and replaced with fresh growth media (4 mL) containing either DMSO (0.05%) or Capzimin (Med Chem Express #HY-110404; 0.05% DMSO, 5 uM compound) and incubated at 37 ˚C, 5% CO_2 for 1 hour. Afterwards, either DMSO (0.05%) or Bortezomib (300 nM, 0.05%) were added directly into the corresponding plate and incubated an additional 24 hours at 37˚C, 5% CO_2. Cells were removed from the plates using Trypsin EDTA (0.25%, 2 mL) and rinsed with PBS (4 mL) before being spun down and the pellets washed with PBS (0.5 mL) before being resuspended in lysis buffer (PBS (8 mL) + EDTA free protease inhibitor (Millipore Sigma #11836170001, 1 tablet), 50-80 µL) and lysed using sonication. The sonicated samples were centrifuged (2000 xg, 20-30 minutes, 4 ˚C) before the supernatant was removed and stored at -80 ˚C. A Pierce protein analysis kit (Thermofisher Scientific #23225) was used to determine the concentration of total protein levels in each sample following the manufacturer's instructions. The samples were analyzed using immunoblotting.

Inhibition of 26S proteasome – siRNAs

HeLa cells (500,000 cells) were plated in 6 well TC-treated plate in growth media (without Normocin or pen/strep, 2 mL) and incubated overnight at 37 ˚C, 5% CO_2. The media was swapped with fresh media (without Normocin or pen/strep) and siRNA transfection occurred as follows: cells were transfected with siRNA knock down of PSMC5 (Thermofisher Scientific, #4390824-s11380) or PSMD11 (Thermofisher Scientific, #4392420-s11413) with Lipofectamine RNAi Max (Thermofisher Scientific, #13778100), diluted in OptiMEM according to vendor protocol and incubated 24 hours at 37 ˚C, 5% CO_2. The next day, Bortezomib samples were dosed directly into the media (0.1% DMSO, 300 nM) and incubated another 24 hours at 37 ˚C, 5% CO_2. Cells were harvested using Trypsin (0.25%, 2 mL), washed with PBS (5 mL) and resuspended in lysis buffer (PBS + protease inhibitor, 50-80 µL) and lysed using sonication. The sonicated samples were centrifuged (2000 xg, 20-30 minutes, 4 ˚C) before the supernatant was removed and stored at -80 ˚C. A Pierce protein analysis kit (Thermofisher Scientific #23225) was used to determine the concentration of total protein levels in each sample following the manufacturer's instructions. The samples were analyzed using immunoblotting.

In-vitro fluorogenic small peptide assay

20S proteasome (R&D systems #E-360, final concentration 1 nM) was prepared in 38 mM Tris-HCl, 100 mM NaCl (pH 7.8) solution and added (89 µL) to each well of a black, flat-bottom, clear-bottom 96-well plate (Corning #3631). Various concentrations of test compound (1 µL) or DMSO alone as the vehicle control were added to each well. After incubation for 15 min at 37 °C, fluorogenic probes suc-LLVY-AMC, Z-LLE-AMC, and Boc-LRR-AMC (R&D systems #S-280, #S-230, #S-300) were added in combination (total concentration 20 µM, 10 µL) was added. Fluorescence was monitored for 1 h at 37 °C using a SpectraMax M5e plate reader at

412 excitation/emission wavelengths of 380/460 nm, and activity was expressed as fluorescence units
413 per minute. Enzymatic activity in compound-treated samples was normalized to that of the
414 vehicle control, and fold change was plotted against the logarithm of compound concentration
415 using GraphPad Prism 9. The 26S proteasome assay followed the same procedure except 26S
416 proteasome solution (R&D systems #E-365, final concentration 1 nM) was prepared in 38 mM
417 Tris-HCl (pH 7.8) containing 2.5 mM ATP-Mg and 5 mM $MgCl_2$.

418 *HPV18+ cellular degradation assay*

419 Cells were plated (1,600,000) in growth media (3 mL) and incubated overnight at 37 ˚C,
420 5% CO_2. The media was removed and replaced with media containing either DMSO (0.1%) or
421 compound at indicated concentrations (4 mL). The samples were incubated for 24 hours at 37 ˚C,
422 5% CO_2. The next day, cells were scraped, diluted in PBS (Thermofisher Scientific #10010023, 6
423 mL) and spun down and the pellets washed with PBS (0.5 mL) before being resuspended in lysis
424 buffer (PBS (8 mL) + EDTA free protease inhibitor (Millipore Sigma #11836170001, 1 tablet),
425 50-80 µL) and lysed using sonication. The sonicated samples were centrifuged (2000 xg, 20-30
426 minutes, 4 ˚C) before the supernatant was removed and stored at -80 ˚C. A Pierce protein
427 analysis kit (Thermofisher Scientific #23225) was used to determine the concentration of total
428 protein levels in each sample following the manufacturer's instructions. The samples were
429 analyzed using immunoblotting (HPV18 E6 and E7) as stated in the above protocol or ELISA
430 (P53: Abcam, Waltham, MA #ab171571) following the manufacturer's instructions.

431 *HPV16+ cellular degradation assay*

432 CaSki cells were plated (750,000 cells/well) in growth media (2 mL) in a 6 well TC-
433 treated plate and incubated overnight at 37˚C, 5% CO_2. The media was removed and replaced

with media (without pen/strep or Normocin; 2 mL) and siRNA transfection was done on the control sample as described in the transfection protocol that follows. 24 hours after transfection started, all samples except siRNA control got fresh media (without pen/strep or Normocin) and compound (indicated concentrations) or DMSO (0.1%) were added directly to the well. The samples were incubated for 24 hours at 37˚C, 5% CO_2. The next day, cells were scraped, diluted in PBS (8 mL) and spun down and the pellets washed with PBS (0.5 mL) before being resuspended in lysis buffer (HPV16 E7 ELISA: RIPA (Thermofisher Scientific #89900) + protease inhibitor; P53 ELISA: ELISA kit lysis buffer + protease inhibitor; 50-80 µL) and lysed according to the manufacturer's protocol. The lysed samples were centrifuged (2000 xg, 20-30 minutes, 4 ˚C) before the supernatant was removed and stored at -80 ˚C. A Pierce BCA protein analysis kit was used to determine the concentration of total protein levels in each sample. The samples were analyzed using ELISA (HPV16 E7: Abcam #ab322427; P53: Abcam #ab171571) following the manufacturer's instructions.

HPV16 E7 siRNA transfection

Prior to transfection, growth media was exchanged with media (without normocin or pen/strep, 2 mL). The transfection cocktail was made combining HPV16 E7 siRNA (Santa Cruz Biotechnology #sc-270423), Xtremegene HP DNA transfection reagent (Milipore Sigma #6366244001), and Optimem (Thermofisher Scientific #31985062) as follows: 1 ug siRNA + 2:1 v:v Xtremegene:siRNA + 100:1 uL Optimem:ug siRNA, combined and incubated at RT for 20 minutes before added directly to the media in the well, dropwise (124 uL) and incubated for 6 hours before media was replaced in that sample with fresh media (without normocin or pen/strep, 2 mL).

Proteasome inhibitor pre-treatment impact on compound cellular effect

HeLa cells were plated (1,600,000 cells/plate) in 6 cm plates in growth media (4 mL) and incubated at 37˚C, 5% CO_2 overnight. The next day, media was replaced with media (4 mL) containing DMSO (0.05%) or proteasome inhibitor Bortezomib (300 nM) and incubated at 37 ˚C, 5% CO_2. After 1 hour, DMSO (2 µL) or compound (2 µL, final concentration = 10 µM) were added directly to the media and incubated at 37 ˚C, 5% CO_2 for an additional 23 hours. Cells were scraped, diluted in PBS (6 mL) and spun down and the pellets washed with PBS (0.5 mL) before being resuspended in PBS + EDTA free protease inhibitor (50-80 µL) and lysed using sonication. The sonicated samples were centrifuged (2000 xg, 20-30 minutes, 4 ˚C) before the supernatant was removed and stored at -80 ˚C. A Pierce BCA protein analysis kit was used to determine the concentration of total protein levels in each sample. The samples were analyzed using immunoblotting.

Quantitative reverse transcriptase polymerase chain reaction (RT-qPCR)

Cellular experiments were performed the same as in described in *HPV18+ and HPV16+ cellular degradation assays*. After the incubation time, cells were pelleted, washed with PBS, and frozen in dry ice before being stored at -80 C. Cells were lysed and RNA isolated using Monarch spin RNA isolation kit (New England Biosciences, Ipswich, MA #T2110S) according to manufacturer's protocol. RNA concentration was determined using a Nanodrop spectrophotometer. RT-qPCR was done using SYBR green Luna universal one-step RT-qPCR kit (New England Biosciences #E3005L) on the isolated RNA (1 ng) using Applied Biosystems 7500Fast Real-Time PCR. Primer sequences listed below (Thermofisher Scientific #10336022):

Oligonucleotide	Sequence 5'-3'	Reference
GAPDH	FOR: TCATTTCCTGGTATGACAACG REV: ATGTGGGCCATGAGGT	Enge, M.; et al. *Cancer Cell* **2009**, *15* (3), 171-183.
HPV16 E6/E7	FOR: ACAAGCAGAACCGGACAGAG REV: GCCCATTAACAGGTCTTCCA	Magaldi, T. G.; et al. *Virology* **2012**, *422* (1), 114-124.
HPV18 E6/E7	FOR: TGAAATTCCGGTTGACCTTC REV: CACGGACACACAAAGGACAG	Magaldi, T. G.; et al. *Virology* **2012**, *422* (1), 114-124.
CDKN1A	FOR: CCATAGCCTCTACTGCCACCATC REV: GTCCAGCGACCTTCCTCATCCA	Wang, L. H.; et al. *Sci Rep* **2016**, *6*, 36486.
TK1	FOR: GCATTAACCTGCCCACTGT REV: CGTCTCATCAACTCTGTGCTTT	Bitter, E. E.; et al. *PLoS One* **2023**, *18* (11), e0293128.

479

480 *Multiplexed viability (cell-titer glo) and toxicity (cell-tox green) HPV+ cellular assays*

481 Cells were plated (5,000 cells/well) in white, clear bottomed, tissue-culture treated, sterile
482 96-well plate in growth media (100 µL) and incubated at 37˚C, 5% CO_2. The next day, the media
483 was removed and replaced with media (100 µL) containing either DMSO (0.1%) or compound
484 (at indicated concentrations). The plates were incubated at 37˚C, 5% CO_2 for 72 hours. After the
485 incubation was over, lysis buffer (1:25 dilution) was added to each lysis sample lane and

incubated for an additional 30 minutes. Then, cell-tox green (Promega, Madison, WI # G874) was added to the plate according to the manufacturer's "endpoint multiplex concentrated reagent addition" instructions and the plate fluorescence read using a plate reader (Ex = 495 nm, Em = 525 nm). The plate was left to equilibrate to RT for 15 minutes. Then, cell-titer glo reagent (Promega, #G8461) was added according to the manufacturer's instructions and luminescence read on a plate reader. The average signal from the lysed samples was used as 100% cell death, while the average signal from the vehicle samples was used as 100% cell viability. The compound treated samples were compared to these signals to calculated % cell death and % cell viability, respectively.

Clonogenic assay

HeLa and CaSki cells (100, 250 cells/well respectively) were plated in growth media (3 mL) in tissue culture treated, sterile, 6 well plates and incubated at 37 ˚C, 5% CO_2 overnight. The next day, DMSO (3 µL) or compound (3 µL, final concentration = 10 µM) was added directly to the media and the plates swirled to mix. The plates were incubated at 37 ˚C, 5% CO_2 for 24 hours before the media was gently replaced with fresh growth media (3 mL). The cells were allowed to incubate at 37˚C, 5% CO_2 for another 14 days (HeLa) or 22 days (CaSki), with media being refreshed occurring every 4-7 days. After the indicated incubation time, cells were fixed using formaldehyde (4% in water, 2 mL/well) and dyed with crystal violet stain (1% crystal violet in 20% EtOH, 2 mL/well) and washed twice, 1x with PBS (2 mL), 1x with water (2 mL). CaSki cells were washed 1x additionally with water (2 mL).

Cell cycle flow cytometry assay

Cells were plated (900,000 HeLa cells; 1,500,000 CaSki cells) were plated in their respective growth medias (8 mL) in T75 TC-treated flasks and incubated at 37 ˚C, 5% CO_2 overnight. The next day, the media was replaced with media + compound or DMSO (0.1% DMSO, 10 mL). The samples were incubated at 37 ˚C, 5% CO_2 for 72 hours. For the positive Thymidine treatment control was given media + DMSO at the time of dosing and incubated for 48 hours. Then, media was replaced with fresh growth media + Thymidine (Sigma Aldrich, Burlington, MA #T1895-1G; 2 mM, 10 mL) and incubated for the remaining 24 hours. After incubation, cells were detached using Trypsin EDTA (0.25%, 5 mL) and diluted in PBS + 2% FBS and counted. 1,000,000 cells were added to each sample tube and fixed with cold 70% EtOH (1 mL) at 4˚C for 1 hour. The cells were washed and stored at 4˚C in PBS (5 mL). Before FACS analysis, the samples were spun down and reconstituted in PBS + FxCycle Violet (Thermofisher Scientific #F10347; 1:1000; 1,000,000 cells/mL) and incubated on ice for 30 minutes. The samples were read using an Attune NxT instrument through the University of Virginia Flow Cytometry Core Facility.

Proteomics cell assay

HeLa cells were plated (3,500,000 cells/plate) in 10 cm TC-treated plates in growth media (10 mL) and incubated at 37 ˚C, 5% CO_2 overnight. The next day, media was replaced with growth media + compound (0.1% DMSO, 10 μM) or DMSO (0.1% DMSO) and incubated at 37 ˚C, 5% CO_2 for 24 hours. The cells were scraped from the plate and rinsed with PBS (4.5 mL), washed 2x with PBS (1 mL then 0.5 mL), before the pellet was resuspended in PBS (80 μL) and lysed via sonication. The lysed samples were spun at 1500 xg for 20 minutes, 4 ˚C, the supernatant was removed and flash frozen in liquid nitrogen (60 seconds) before storage at -80 ˚C.

Whole cell proteomics

Protein concentrations were measured using Pierce BCA assay kit. Subsequently, proteins were reduced with 5 mM TCEP for 15 minutes, alkylated with 15 mM iodoacetamide in the dark for 30 minutes, and quenched with 10 mM DTT at room temperature. After that, the proteins were digested overnight at 37 ˚C with Lys-C and trypsin. The samples were then desalted, dried and resuspended in 5% acetonitrile and 5% formic acid for mass spectrometry analysis. Equal amounts of sample were injected for all runs.

Liquid chromatography: Peptide separation was carried out on a Vanquish Neo UHPLC system using a trap-and-elute setup. An Aurora Frontier™ TS C18 column (IonOpticks, 60 cm length/75 µm inner diameter/1.7 µm particle size) was used for peptide separation. The mobile phases used were: Phase A — 0.1% formic acid (FA) in water; Phase B — 80% acetonitrile (ACN) with 0.1% FA in water. A 50-min active gradient ramped, at a flow rate of 0.3 µl/min, from 12 to 18% MPB from 0.1 to 8 min, 18 to 45% MPB from 8 to 50 min at a flow rate of 0.2 µl/min, 45 to 99% MPB from 50 to 50.1min, and held at 99% MPB to 15 min before the column was washed and re-equilibrated at 1% MPB for 35 min.

Mass spectrometry data acquisition: Data were acquired using an Orbitrap Astral mass spectrometer in a DIA mode. MS1 spectra were acquired at a resolution of 240,000 over an m/z range of 380–980. The MS1 normalized AGC target was set to 250%, and the maximum injection time was set to 50 ms. DIA MS2 scans were recorded at a resolution of 80,000 with a normalized AGC target of 500%. The HCD normalized collision energy was set to 25%, and a 0.6 s cycle time was used with a maximum injection time of 3.5 ms and a 2 Th isolation window. Equal amounts of sample were injected for all runs.

552 DIA data analysis: DIA raw files were searched using Spectronaut (version 19.6.250122.62635)
553 with the default directDIA settings and a human reference proteome database (UniProt release
554 2024-12-19; 83,405 entries). For Pulsar search settings, Trypsin/P was selected as the digestion
555 enzyme with up to two missed cleavages. Carbamidomethyl (C) was specified as a fixed
556 modification, while Acetyl (Protein N-term) and Oxidation (M) were included as variable
557 modifications. In the Result Filters settings, the Top3–6 best fragments per peptide were used.

558 For DIA analysis settings, in the Identification panel, the precursor q-value and
559 experiment-wide protein q-value thresholds were set to 0.01, and the run-wise protein q-value
560 threshold was set to 0.05. In the Quantification panel, quantification was performed at the MS2
561 level, and cross-run normalization was enabled. Peptide and protein quantities were summarized
562 using a maximum of Top 3 precursors and Top 3 striped peptide sequences, respectively.
563 PG.Quantity values are exported for each protein quantitation.

564 *Proteomics pathway analysis*

565 The count matrix was used as the input for differential proteomics analysis. The R
566 package DEqMS[53] was used to perform the analysis. Lowly expressed proteins were filtered out
567 prior to the analysis. Protein counts were $\log_2$-transformed, followed by median sweeping to
568 center the median expression of each sample at zero. The following two contrasts were analyzed:
569 TCH-165 vs. vehicle control and MM treatment vs. vehicle control. For each contrast, volcano
570 plots representing significantly upregulated and downregulated proteins were generated using
571 functions available in the DEqMS package.

572 Pathway enrichment analysis was performed using the R package clusterProfiler[68] and
573 the MSigDB pathway reference database Hallmark gene sets.[54, 69, 70]

Statistical analysis

All values are expressed as a mean ± standard deviation, with the individual biological replicates plotted as symbols in bar graphs. The number of biological replicates is indicated in the data figure caption; every experiment was repeated at least three times. No pre-determination of sample size was done prior to experimentation. The statistical analyses used are indicated in the data figure captions. Normality of dataset residuals was tested using the Shapiro-Wilk test and Quantile-Quantile (Q-Q) graph visual verification. The ROUT method was used to determine if outliers could be removed (Q=1%). Variance was measured using the Brown-Forsythe test. The appropriate statistical test was used for each data set according to determination of its variance and normality. Statistical analysis was done using Graphpad Prism ().

Data Availability

The proteomics datasets generated and analyzed during the current study will be deposited in the ProteomeXchange Consortium repository via PRIDE prior to publication. Accession numbers will be included in the final published version of the manuscript. All other data supporting the findings of this study are available within the paper and Supplementary Information.

References

(1) Dash, S. R.; Kundu, A.; Kundu, C. N. The role of viruses in cancer progression versus cancer treatment: A dual paradigm. *Life Sciences* **2024**, *341*, 122506. DOI: 10.1016/j.lfs.2024.122506.

(2) Basukala, O.; Banks, L. The Not-So-Good, the Bad and the Ugly: HPV E5, E6 and E7 Oncoproteins in the Orchestration of Carcinogenesis. *Viruses* **2021**, *13*. DOI: 10.3390/v13101892.

(3) Pal, A.; Kundu, R. Human Papillomavirus E6 and E7: The Cervical Cancer Hallmarks and Targets for Therapy. *Frontiers in Microbiology* **2020**, *10*, Review. DOI: 10.3389/fmicb.2019.03116.

(4) Yeo-Teh, N. S. L.; Ito, Y.; Jha, S. High-Risk Human Papillomaviral Oncogenes E6 and E7 Target Key Cellular Pathways to Achieve Oncogenesis. *International Journal of Molecular Sciences* **2018**, *19* (6), 1706. DOI: 10.3390/ijms19061706.

(5) WHO. *Immunization coverage*. World Health Organization, 2026. https://www.who.int/news-room/fact-sheets/detail/immunization-coverage.

(6) Uversky, V. N.; Roman, A.; Oldfield, C. J.; Dunker, A. K. Protein Intrinsic Disorder and Human Papillomaviruses: Increased Amount of Disorder in E6 and E7 Oncoproteins from High Risk HPVs. *Journal of Proteome Research* **2006**, *5* (8), 1829-1842. DOI: 10.1021/pr0602388.

(7) Calçada, E. O.; Felli, I. C.; Hošek, T.; Pierattelli, R. The Heterogeneous Structural Behavior of E7 from HPV16 Revealed by NMR Spectroscopy. *ChemBioChem* **2013**, *14* (14), 1876-1882. DOI: 10.1002/cbic.201300172.

(8) Kukic, P.; Lo Piccolo, G. M.; Nogueira, M. O.; Svergun, D. I.; Vendruscolo, M.; Felli, I. C.; et al. The free energy landscape of the oncogene protein E7 of human papillomavirus type 16 reveals a complex interplay between ordered and disordered regions. *Scientific Reports* **2019**, *9* (1), 5822. DOI: 10.1038/s41598-019-41925-4.

(9) Arizmendi-Izazaga, A.; Navarro-Tito, N.; Jiménez-Wences, H.; Evaristo-Priego, A.; Priego-Hernández, V. D.; Dircio-Maldonado, R.; et al. Bioinformatics Analysis Reveals E6 and E7 of

HPV 16 Regulate Metabolic Reprogramming in Cervical Cancer, Head and Neck Cancer, and Colorectal Cancer through the PHD2-VHL-CUL2-ELOC-HIF-1α Axis. *Current Issues in Molecular Biology* **2024**, *46* (6), 6199-6222. DOI: 10.3390/cimb46060370.

(10) Sitarz, K.; Czamara, K.; Szostek, S.; Kaczor, A. The impact of HPV infection on human glycogen and lipid metabolism – a review. *Biochimica et Biophysica Acta (BBA) - Reviews on Cancer* **2022**, *1877* (1), 188646. DOI: 10.1016/j.bbcan.2021.188646.

(11) De Leon-Oliva, D.; González-Prieto, P.; De Castro-Martinez, P.; Boaru, D. L.; Laguna-Hernández, P.; Fraile-Martinez, O.; et al. Revisiting the biological role of the Warburg effect: Evolving perspectives on cancer metabolism. *Pathology - Research and Practice* **2025**, *273*, 156151. DOI: 10.1016/j.prp.2025.156151.

(12) Gore, M.; Kabekkodu, S. P.; Chakrabarty, S. Exploring the metabolic alterations in cervical cancer induced by HPV oncoproteins: From mechanisms to therapeutic targets. *Biochimica et Biophysica Acta (BBA) - Reviews on Cancer* **2025**, *1880* (2), 189292. DOI: 10.1016/j.bbcan.2025.189292.

(13) Pappa, K. I.; Daskalakis, G.; Anagnou, N. P. Metabolic rewiring is associated with HPV-specific profiles in cervical cancer cell lines. *Scientific Reports* **2021**, *11* (1), 17718. DOI: 10.1038/s41598-021-96038-8.

(14) Hu, C.; Liu, T.; Han, C.; Xuan, Y.; Jiang, D.; Sun, Y.; et al. HPV E6/E7 promotes aerobic glycolysis in cervical cancer by regulating IGF2BP2 to stabilize m⁶A-MYC expression. *International Journal of Biological Sciences* **2022**, *18* (2), 507-521. DOI: 10.7150/ijbs.67770.

(15) Wang, L.; Li, X.; Ren, C.; Liu, L.; Yao, J.; Wu, M.; et al. Site-specific HPV18 integration facilitates cervical carcinogenesis through metabolic reprogramming-induced dysfunction of the

SpHK1/S1P/S1PR1 pathway. *Cell Death & Disease* **2026**, *17* (1), 24. DOI: 10.1038/s41419-025-08195-7.

(16) Liu, J.; Huang, B.; Xiu, Z.; Zhou, Z.; Liu, J.; Li, X.; et al. PI3K/Akt/HIF-1α signaling pathway mediates HPV-16 oncoprotein-induced expression of EMT-related transcription factors in non-small cell lung cancer cells. *J Cancer* **2018**, *9* (19), 3456-3466. DOI: 10.7150/jca.26112.

(17) Lee, M. Y.; Shen, M. R. Epithelial-mesenchymal transition in cervical carcinoma. *Am J Transl Res* **2012**, *4* (1), 1-13. DOI: 10.1158/1078-0432.CCR-08-0234.

(18) Chung, M.-T.; Lai, H.-C.; Sytwu, H.-K.; Yan, M.-D.; Shih, Y.-L.; Chang, C.-C.; et al. SFRP1 and SFRP2 suppress the transformation and invasion abilities of cervical cancer cells through Wnt signal pathway. *Gynecologic Oncology* **2009**, *112* (3), 646-653. DOI: 10.1016/j.ygyno.2008.10.026.

(19) Li, J.; Zhou, B. P. Activation of β-catenin and Akt pathways by Twist are critical for the maintenance of EMT associated cancer stem cell-like characters. *BMC Cancer* **2011**, *11* (1), 49. DOI: 10.1186/1471-2407-11-49.

(20) Zhou, Z.; Wu, X.; Zhan, R.; Li, X.; Cheng, D.; Chen, L.; et al. Exosomal epidermal growth factor receptor is involved in HPV-16 E7-induced epithelial-mesenchymal transition of non-small cell lung cancer cells: A driver of signaling in vivo. *Cancer Biology & Therapy* **2022**, *23* (1), 1-13. DOI: 10.1080/15384047.2022.2133332.

(21) Zhang, W.; Wu, X.; Hu, L.; Ma, Y.; Xiu, Z.; Huang, B.; et al. Overexpression of Human Papillomavirus Type 16 Oncoproteins Enhances Epithelial-Mesenchymal Transition via STAT3 Signaling Pathway in Non-Small Cell Lung Cancer Cells. *Oncol Res* **2017**, *25* (5), 843-852. DOI: 10.3727/096504016x14813880882288.

(22) Wang, M.; Qiao, X.; Cooper, T.; Pan, W.; Liu, L.; Hayball, J.; et al. HPV E7-mediated NCAPH ectopic expression regulates the carcinogenesis of cervical carcinoma via PI3K/AKT/SGK pathway. *Cell Death & Disease* **2020**, *11* (12), 1049. DOI: 10.1038/s41419-020-03244-9.

(23) Njomen, E.; Tepe, J. J. Proteasome Activation as a New Therapeutic Approach To Target Proteotoxic Disorders. *Journal of Medicinal Chemistry* **2019**, *62* (14), 6469-6481. DOI: 10.1021/acs.jmedchem.9b00101.

(24) Ruan, H.; Sun, Q.; Zhang, W.; Liu, Y.; Lai, L. Targeting intrinsically disordered proteins at the edge of chaos. *Drug Discovery Today* **2019**, *24* (1), 217-227. DOI: 10.1016/j.drudis.2018.09.017.

(25) Njomen, E.; Osmulski, P. A.; Jones, C. L.; Gaczynska, M.; Tepe, J. J. Small Molecule Modulation of Proteasome Assembly. *Biochemistry* **2018**, *57* (28), 4214-4224. DOI: 10.1021/acs.biochem.8b00579.

(26) Fabre, B.; Lambour, T.; Garrigues, L.; Ducoux-Petit, M.; Amalric, F.; Monsarrat, B.; et al. Label-Free Quantitative Proteomics Reveals the Dynamics of Proteasome Complexes Composition and Stoichiometry in a Wide Range of Human Cell Lines. *Journal of Proteome Research* **2014**, *13* (6), 3027-3037. DOI: 10.1021/pr500193k.

(27) Tanahashi, N.; Murakami, Y.; Minami, Y.; Shimbara, N.; Hendil, K. B.; Tanaka, K. Hybrid Proteasomes: INDUCTION BY INTERFERON-γ AND CONTRIBUTION TO ATP-DEPENDENT PROTEOLYSIS*. *Journal of Biological Chemistry* **2000**, *275* (19), 14336-14345. DOI: 10.1074/jbc.275.19.14336.

(28) Thrower, J. S. Recognition of the polyubiquitin proteolytic signal. *The EMBO Journal* **2000**, *19* (1), 94-102. DOI: 10.1093/emboj/19.1.94.

(29) George, D. E.; Tepe, J. J. Advances in Proteasome Enhancement by Small Molecules. *Biomolecules* **2021**, *11* (12), 1789. DOI: 10.3390/biom11121789.

(30) Martinez-Fonts, K.; Davis, C.; Tomita, T.; Elsasser, S.; Nager, A. R.; Shi, Y.; et al. The proteasome 19S cap and its ubiquitin receptors provide a versatile recognition platform for substrates. *Nature Communications* **2020**, *11* (1), 477. DOI: 10.1038/s41467-019-13906-8.

(31) Kumar Deshmukh, F.; Yaffe, D.; Olshina, M. A.; Ben-Nissan, G.; Sharon, M. The Contribution of the 20S Proteasome to Proteostasis. *Biomolecules* **2019**, *9* (5), 190. DOI: 10.3390/biom9050190.

(32) García-Alai, M. M.; Alonso, L. G.; de Prat-Gay, G. The N-Terminal Module of HPV16 E7 Is an Intrinsically Disordered Domain That Confers Conformational and Recognition Plasticity to the Oncoprotein. *Biochemistry* **2007**, *46* (37), 10405-10412. DOI: 10.1021/bi7007917.

(33) Njomen, E.; Vanecek, A.; Lansdell, T. A.; Yang, Y.-T.; Schall, P. Z.; Harris, C. M.; et al. Small Molecule 20S Proteasome Enhancer Regulates MYC Protein Stability and Exhibits Antitumor Activity in Multiple Myeloma. *Biomedicines* **2022**, *10* (5), 938. DOI: 10.3390/biomedicines10050938.

(34) Staerz, S. D.; Anamoah, C.; Tepe, J. J. 20S proteasome enhancers prevent cytotoxic tubulin polymerization-promoting protein induced α-synuclein aggregation. *iScience* **2024**, *27* (7). DOI: 10.1016/j.isci.2024.110166.

(35) Vanecek, A. S.; Mojsilovic-Petrovic, J.; Kalb, R. G.; Tepe, J. J. Enhanced Degradation of Mutant C9ORF72-Derived Toxic Dipeptide Repeat Proteins by 20S Proteasome Activation Results in Restoration of Proteostasis and Neuroprotection. *ACS Chemical Neuroscience* **2023**, *14* (8), 1439-1448. DOI: 10.1021/acschemneuro.2c00732.

(36) Yun, H.-Y.; Kim, M. W.; Lee, H. S.; Kim, W.; Shin, J. H.; Kim, H.; et al. Structural basis for recognition of the tumor suppressor protein PTPN14 by the oncoprotein E7 of human papillomavirus. *PLOS Biology* **2019**, *17* (7), e3000367. DOI: 10.1371/journal.pbio.3000367.

(37) Mauvezin, C.; Neufeld, T. P. Bafilomycin A1 disrupts autophagic flux by inhibiting both V-ATPase-dependent acidification and Ca-P60A/SERCA-dependent autophagosome-lysosome fusion. *Autophagy* **2015**, *11* (8), 1437-1438. DOI: 10.1080/15548627.2015.1066957.

(38) Zhang, W.; Che, Q.; Tan, H.; Qi, X.; Li, J.; Li, D.; et al. Marine Streptomyces sp. derived antimycin analogues suppress HeLa cells via depletion HPV E6/E7 mediated by ROS-dependent ubiquitin–proteasome system. *Scientific Reports* **2017**, *7* (1), 42180. DOI: 10.1038/srep42180.

(39) Kehmeier, E.; Rühl, H.; Voland, B.; Conrad Stöppler, M.; Androphy, E.; Stöppler, H. Cellular Steady-State Levels of "High Risk" but Not "Low Risk" Human Papillomavirus (HPV) E6 Proteins Are Increased by Inhibition of Proteasome-Dependent Degradation Independent of Their p53- and E6AP-Binding Capabilities. *Virology* **2002**, *299* (1), 72-87. DOI: 10.1006/viro.2002.1502.

(40) Teicher, B. A.; Ara, G.; Herbst, R.; Palombella, V. J.; Adams, J. The Proteasome Inhibitor PS-341 in Cancer Therapy. *Clinical Cancer Research* **1999**, *5* (9), 2638-2645.

(41) Li, J.; Yakushi, T.; Parlati, F.; Mackinnon, A. L.; Perez, C.; Ma, Y.; et al. Capzimin is a potent and specific inhibitor of proteasome isopeptidase Rpn11. *Nat Chem Biol* **2017**, *13* (5), 486-493. DOI: 10.1038/nchembio.2326.

(42) de Poot, S. A. H.; Tian, G.; Finley, D. Meddling with Fate: The Proteasomal Deubiquitinating Enzymes. *Journal of Molecular Biology* **2017**, *429* (22), 3525-3545. DOI: 10.1016/j.jmb.2017.09.015.

(43) Yu, Z.-Q.; Carmichael, J.; Collins, G. A.; D'Agostino, M. D.; Lessard, M.; Firth, H. V.; et al. PSMC5 insufficiency and P320R mutation impair proteasome function. *Human Molecular Genetics* **2024**, *33* (17), 1506-1523. DOI: 10.1093/hmg/ddae085.

(44) Sokolova, V.; Li, F.; Polovin, G.; Park, S. Proteasome Activation is Mediated via a Functional Switch of the Rpt6 C-terminal Tail Following Chaperone-dependent Assembly. *Scientific Reports* **2015**, *5* (1), 14909. DOI: 10.1038/srep14909.

(45) Pathare, G. R.; Nagy, I.; Bohn, S.; Unverdorben, P.; Hubert, A.; Körner, R.; et al. The proteasomal subunit Rpn6 is a molecular clamp holding the core and regulatory subcomplexes together. *Proceedings of the National Academy of Sciences* **2012**, *109* (1), 149-154. DOI: 10.1073/pnas.1117648108.

(46) Deb, W.; Rosenfelt, C.; Vignard, V.; Papendorf, J. J.; Möller, S.; Wendlandt, M.; et al. PSMD11 loss-of-function variants correlate with a neurobehavioral phenotype, obesity, and increased interferon response. *The American Journal of Human Genetics* **2024**, *111* (7), 1352-1369. DOI: 10.1016/j.ajhg.2024.05.016.

(47) Ben-Saadon, R.; Fajerman, I.; Ziv, T.; Hellman, U.; Schwartz, A. L.; Ciechanover, A. The tumor suppressor protein p16(INK4a) and the human papillomavirus oncoprotein-58 E7 are naturally occurring lysine-less proteins that are degraded by the ubiquitin system. Direct evidence for ubiquitination at the N-terminal residue. *J Biol Chem* **2004**, *279* (40), 41414-41421. DOI: 10.1074/jbc.M407201200.

(48) Staerz, S. D.; Lisabeth, E. M.; Njomen, E.; Dexheimer, T. S.; Neubig, R. R.; Tepe, J. J. Development of a Cell-Based AlphaLISA Assay for High-Throughput Screening for Small Molecule Proteasome Modulators. *ACS Omega* **2023**, *8* (17), 15650-15659. DOI: 10.1021/acsomega.3c01158.

(49) Engeland, K. Cell cycle regulation: p53-p21-RB signaling. *Cell Death & Differentiation* **2022**, *29* (5), 946-960. DOI: 10.1038/s41418-022-00988-z.

(50) DeCaprio, J. A. Human papillomavirus type 16 E7 perturbs DREAM to promote cellular proliferation and mitotic gene expression. *Oncogene* **2014**, *33* (31), 4036-4038. DOI: 10.1038/onc.2013.449.

(51) Mandigo, A. C.; Tomlins, S. A.; Kelly, W. K.; Knudsen, K. E. Relevance of pRB Loss in Human Malignancies. *Clinical Cancer Research* **2022**, *28* (2), 255-264. DOI: 10.1158/1078-0432.CCR-21-1565.

(52) Goodwin, E. C.; DiMaio, D. Repression of human papillomavirus oncogenes in HeLa cervical carcinoma cells causes the orderly reactivation of dormant tumor suppressor pathways. *Proceedings of the National Academy of Sciences* **2000**, *97* (23), 12513-12518. DOI: 10.1073/pnas.97.23.12513.

(53) Zhu, Y.; Orre, L. M.; Zhou Tran, Y.; Mermelekas, G.; Johansson, H. J.; Malyutina, A.; et al. DEqMS: A Method for Accurate Variance Estimation in Differential Protein Expression Analysis. *Mol Cell Proteomics* **2020**, *19* (6), 1047-1057. DOI: 10.1074/mcp.TIR119.001646.

(54) Liberzon, A.; Birger, C.; Thorvaldsdóttir, H.; Ghandi, M.; Mesirov, J. P.; Tamayo, P. The Molecular Signatures Database (MSigDB) hallmark gene set collection. *Cell Syst* **2015**, *1* (6), 417-425. DOI: 10.1016/j.cels.2015.12.004.

(55) Beaudenon, S.; Huibregtse, J. M. HPV E6, E6AP and cervical cancer. *BMC Biochem* **2008**, *9 Suppl 1* (Suppl 1), S4. DOI: 10.1186/1471-2091-9-s1-s4.

(56) Taylor, W. R.; Stark, G. R. Regulation of the G2/M transition by p53. *Oncogene* **2001**, *20* (15), 1803-1815. DOI: 10.1038/sj.onc.1204252.

(57) Koivusalo, R.; Mialon, A.; Pitkänen, H.; Westermarck, J.; Hietanen, S. Activation of p53 in Cervical Cancer Cells by Human Papillomavirus E6 RNA Interference Is Transient, but Can Be Sustained by Inhibiting Endogenous Nuclear Export–Dependent p53 Antagonists. *Cancer Research* **2006**, *66* (24), 11817-11824. DOI: 10.1158/0008-5472.Can-06-2185.

(58) Koivusalo, R.; Krausz, E.; Helenius, H.; Hietanen, S. Chemotherapy Compounds in Cervical Cancer Cells Primed by Reconstitution of p53 Function after Short Interfering RNA-Mediated Degradation of Human Papillomavirus 18 E6 mRNA: Opposite Effect of siRNA in Combination with Different Drugs. *Molecular Pharmacology* **2005**, *68* (2), 372-382. DOI: 10.1124/mol.105.011189.

(59) Peng, Q.; Wang, L.; Zuo, L.; Gao, S.; Jiang, X.; Han, Y.; et al. HPV E6/E7: insights into their regulatory role and mechanism in signaling pathways in HPV-associated tumor. *Cancer Gene Therapy* **2024**, *31* (1), 9-17. DOI: 10.1038/s41417-023-00682-3.

(60) Kennedy, E. M.; Kornepati, A. V. R.; Goldstein, M.; Bogerd, H. P.; Poling, B. C.; Whisnant, A. W.; et al. Inactivation of the Human Papillomavirus E6 or E7 Gene in Cervical Carcinoma Cells by Using a Bacterial CRISPR/Cas RNA-Guided Endonuclease. *Journal of Virology* **2014**, *88* (20), 11965-11972. DOI: doi:10.1128/jvi.01879-14.

(61) DeFilippis, R. A.; Goodwin, E. C.; Wu, L.; DiMaio, D. Endogenous human papillomavirus E6 and E7 proteins differentially regulate proliferation, senescence, and apoptosis in HeLa cervical carcinoma cells. *J Virol* **2003**, *77* (2), 1551-1563. DOI: 10.1128/jvi.77.2.1551-1563.2003.

(62) Zhang, Y.; Qiu, K.; Ren, J.; Zhao, Y.; Cheng, P. Roles of human papillomavirus in cancers: oncogenic mechanisms and clinical use. *Signal Transduction and Targeted Therapy* **2025**, *10* (1), 44. DOI: 10.1038/s41392-024-02083-w.

798 (63) Contreras-Paredes, A.; De la Cruz-Hernández, E.; Martínez-Ramírez, I.; Dueñas-González,
799 A.; Lizano, M. E6 variants of human papillomavirus 18 differentially modulate the protein
800 kinase B/phosphatidylinositol 3-kinase (akt/PI3K) signaling pathway. *Virology* **2009**, *383* (1), 78-
801 85. DOI: 10.1016/j.virol.2008.09.040.
802 (64) Pim, D.; Massimi, P.; Dilworth, S. M.; Banks, L. Activation of the protein kinase B pathway
803 by the HPV-16 E7 oncoprotein occurs through a mechanism involving interaction with PP2A.
804 *Oncogene* **2005**, *24* (53), 7830-7838. DOI: 10.1038/sj.onc.1208935.
805 (65) Spangle, J. M.; Münger, K. The Human Papillomavirus Type 16 E6 Oncoprotein Activates
806 mTORC1 Signaling and Increases Protein Synthesis. *Journal of Virology* **2010**, *84* (18), 9398-
807 9407. DOI: 10.1128/jvi.00974-10.
808 (66) Cruz-Gregorio, A.; Aranda-Rivera, A. K.; Ortega-Lozano, A. J.; Pedraza-Chaverri, J.;
809 Mendoza-Hoffmann, F. Lipid metabolism and oxidative stress in HPV-related cancers. *Free*
810 *Radical Biology and Medicine* **2021**, *172*, 226-236. DOI: 10.1016/j.freeradbiomed.2021.06.009.
811 (67) Dalamaga, M.; Christodoulatos, G. S.; Liu, J. Diverting epithelial-to-mesenchymal
812 transition to transform cancer cells to adipocytes: A promising strategy to stop metastasis.
813 *Metabolism Open* **2019**, *3*, 100012. DOI: 10.1016/j.metop.2019.100012.
814 (68) Wu, T.; Hu, E.; Xu, S.; Chen, M.; Guo, P.; Dai, Z.; et al. clusterProfiler 4.0: A universal
815 enrichment tool for interpreting omics data. *Innovation (Camb)* **2021**, *2* (3), 100141. DOI:
816 10.1016/j.xinn.2021.100141.
817 (69) Liberzon, A. A description of the Molecular Signatures Database (MSigDB) Web site.
818 *Methods Mol Biol* **2014**, *1150*, 153-160. DOI: 10.1007/978-1-4939-0512-6_9.

(70) Liberzon, A.; Subramanian, A.; Pinchback, R.; Thorvaldsdottir, H.; Tamayo, P.; Mesirov, J. P. Molecular signatures database (MSigDB) 3.0. *Bioinformatics* **2011**, *27* (12), 1739-1740. DOI: 10.1093/bioinformatics/btr260.

Figure Legends

Figure 1: The 20S proteasome alone can degrade HPV18 E6 and E7. (A) In-vitro studies were done with purified 20S proteasome and HPV18 E7 showing that the 20S proteasome is capable of degrading E7. Western blot is representative of three independent experiments. Bar graph shows the average % protein remaining compared to the E7 only sample and error bars represent the standard deviation (SD) from three independent experiments. **(B)** Bafilomycin (500 nM) was used to inhibit autophagy in HPV18+ HeLa cells and western blotting was used to measure the impact on HPV18 E7 levels. Bar graph shows the average % protein remaining compared to the untreated vehicle and error bars represent SD from four independent experiments. Due to data set lacking normality, a Kruskal-Wallis test was done on the $\log_{10}(Y)$ transform of the HPV E6 data which found that the differences between treatments to be not-significant (ns). **(C)** 26S proteasome function was inhibited utilizing either Capzimin (treatment A) or siRNA for the PSMC5 (treatment B) or PSMD11 (treatment C) subunits of the 19S cap. 26S proteasome function was measured through western blotting for K48 polyubiquitinylated protein levels. Western blotting was also used to measure the impact on HPV18 E6 and E7. Western blots are representative of three (treatments B, C) or four (treatment A) independent experiments. Bar graph shows the average % protein compared to untreated vehicles and the error bars represent the SD of three (treatments B, C) or four (treatment A) independent experiments. Due to the data set having variance in SDs, a Welch ANOVA test was done on the $\log_{10}(Y)$ transform of the Capzimin HPV18 E7 data followed by a Dunnett's T3 comparison between the vehicle and each treatment sample. Due to data set lacking normality, a Kruskal-Wallis test was done on the $\log_{10}(Y)$ transform of the PSMD11 siRNA HPV18 E7 data followed by Dunn's multiple comparison test between the vehicle and treatment samples. One-Way

847 ANOVA found both siRNA data set differences to be non-significant in respect to HPV18 E6.
848 Statistical Analysis: Unless specified otherwise, one-way ANOVA was done on the $\log_{10}(Y)$
849 transform of the data followed by Dunnett's multiple comparison test between the vehicle and
850 each treatment sample. *p<0.05, **p<0.01, ***p<0.001, ****p<0.0001, no * = not significant
851 (ns). * p<0.05, ** p<0.01, no stars = not significant. Western blots were cropped for clarity, see
852 the supplementary information for unaltered blots.

853

854 **Figure 2: 20S-proteasome specific enhancers decrease HPV E6 and E7 in a proteasome**
855 **dependent and transcription-independent manner. (A)** Structures of TCH-165 and MM. **(B)**
856 The 20S and 26S proteasome enhancement activities of MM and TCH-165 were analyzed using
857 an *in-vitro* fluorogenic small peptide assay. Graph compares the % change of each compound
858 treatment compared to the untreated vehicle across concentrations of compound as a mean of
859 three independent experiments; error bars represent the SD. **(C)** HPV18+ HeLa cells were treated
860 with MM or TCH-165 for 24 hours, and protein levels were quantified using western blot. Bar
861 graph represents the mean of three (5 μM concentrations) or five (10 μM concentrations, BTZ)
862 independent experiments; the error bars represent the SD. **(D)** HPV16+ CaSki cells were treated
863 with MM or TCH-165 for 24 hours, and protein levels were quantified using HPV16 E7 ELISA.
864 Bar graph represents the mean of three independent experiments (six for vehicle, siRNA); the
865 error bars represent the SD. **(E)** HPV18+ HeLa cells were pre-treated with proteasome inhibitor
866 BTZ for 1 hour before TCH-165 or MM treatment for an additional 23 hours. Bar graph
867 represents the mean of three independent experiments; the error bars represent the SD. **(F)** RT-
868 qPCR was done on RNA purified from HPV18+ HeLa cells treated with TCH-165 or MM (10
869 μM) for 24 hours. Bar graph represents the mean $\log_2$(fold change) of three independent

experiments; the error bars represent the SD. One-way ANOVA test found data set differences to be ns. Statistical analyses: Unless stated otherwise, one-way ANOVA was done on the $\log_{10}(Y)$ transform of the data followed by Dunnett's multiple comparison test between the vehicle and each treatment sample. *p<0.05, **p<0.01, ***p<0.001, ****p<0.0001, no * = not significant (ns). Western blots were cropped for clarity; see the supplementary information for unaltered blots.

Figure 3: 20S proteasome enhancement inhibits HPV+ proliferation by stalling the cell cycle. (A) HPV16+ CaSki cells were treated with each proteasome enhancer (10 μM) for 24 hours and the p53 levels in each sample measured using a p53 ELISA. Bar graph represents the mean of three independent experiments. Error bars represent the SD. **(B)** RT-qPCR was done on HPV18+ HeLa and HPV16+ CaSki cells after treatment with TCH-165 or MM (10 μM) for 24 hours. Bar graph represents the mean $\log_2$(fold change), and the error bars represent the SD of three independent experiments. One-way ANOVA on the $\log_2$(fold change) found both TK1 data set differences to be ns. **(C)** TCH-165 and MM were evaluated for effects on HPV18+ and HPV16+ cell growth using Cell-Titer Glo proliferation and Cell-Tox Green toxicity assays after 72 hours of treatment with varying concentrations of compound. Graph represents % change in signal in proliferation (left y-axis) and toxicity (right y-axis) compared to untreated cells for each concentration of compound tested as a mean of three independent experiments. The error bars represent SD. **(D)** Clonogenic assays were done on HPV18+ and HPV16+ cells treated with BTZ, TCH-165, or MM for 24 hours before media was replaced and cells grown for another 15 days (HPV18+) or 22 days (HPV16+). Images are representative of three individual experiments. **(E)** Compound effect on cell cycle distribution of HPV18+ HeLa and **(F)** HPV16+ CaSki cells

after 72 hours of incubation was assessed using FxCycle Violet flow cytometry dye. Bar graphs represent the mean of three independent experiment % distribution for G0/1, S, and G2/M phases; the error bars represent the SD. One-way ANOVA was done on the data sets followed by Dunnett's multiple comparison test between the vehicle and each treatment sample. Histograms shown are one representation of three independent experiments. Statistical analyses: Unless stated otherwise, one-way ANOVA was done on the $\log_{10}(Y)$ transform of the data followed by Dunnett's multiple comparison test between the vehicle and each treatment sample. *p<0.05, **p<0.01, ***p<0.001, ****p<0.0001, no * = not significant (ns).

Figure 4: TCH-165 and MM impact on HPV18+ global proteome. (A) Bar graph shows the number of proteins identified per sample as a mean of three independent experiments. **(B)** Volcano plots show HPV18+ HeLa cell proteins impacted by TCH-165 or MM treatment comparing $\log_2$(fold change) to -log(adjusted pvalue), and all values are the mean of three independent experiments. **(C)** Gene Set Enrichment pathway analysis bar chart shows pathways impacted by TCH-165 or MM treatment with corresponding enrichment score and q-value. **(D)** Cellular pathways impacted by TCH-165 or MM treatment. Bar graph shows the $\log_2$(fold change) of the specific proteins (idenfitied by their gene codes) in each pathway which were altered by >50%. Values are a mean of three independent experiments.

Acknowledgements

This research uses the HeLa cell line. We acknowledge Mrs. Henrietta Lacks and the HeLa cell line that was established from her tumor cells without her knowledge or consent in 1951, which have made significant contributions to scientific progress and advances in human health. We are grateful to Mrs. Henrietta Lacks, now deceased, and to her surviving family members for their contributions to biomedical research.

The data for this manuscript were generated in the University of Virginia Flow Cytometry Core Facility (RRid:SCR_017829) and is partially supported by the NCI Grant (P30-CA044579). We acknowledge support from the Bioinformatics Core, RRID:SCR_012718. We'd like to thank Dr. Sydney Cobb for editorial support. We'd also like to thank Dr. Heidi Seears and the University of Virginia Department of Biology Genomics Core Facility for training and the use of their instrumentation. We also kindly thank the University of Virginia Biomolecular Magnetic Resonance Facility and the University of Virginia Drug Discovery Core for the use of their instruments.

Funding

We gratefully acknowledge the University of Virginia Comprehensive Cancer Center (P30CA044579) for their financial support.

Conflict of Interest

J.J.T. is a founder of Portera Therapeutics and holds equity in the company. Portera Therapeutics has interests in the development of proteasome-modulating therapeutics. This relationship has been reviewed and managed by the University of Virginia in accordance with its conflict-of-interest policies. All other authors declare no competing interests.

Authors' Contributions

SMC and JJT performed study conceptualization. SMC and LTL designed experiments. SMC, LTL, AC, KAH, BG, and YD performed experiments and analyzed data. GK and PK did data analysis and interpretation. TZ, PK, and JJT provided project supervision. JJT provided funding. SMC drafted the original manuscript with major edits by JJT. LTL, AC, BG, YD, and PK reviewed and edited the manuscript. All authors read and approved the final paper.

Figures

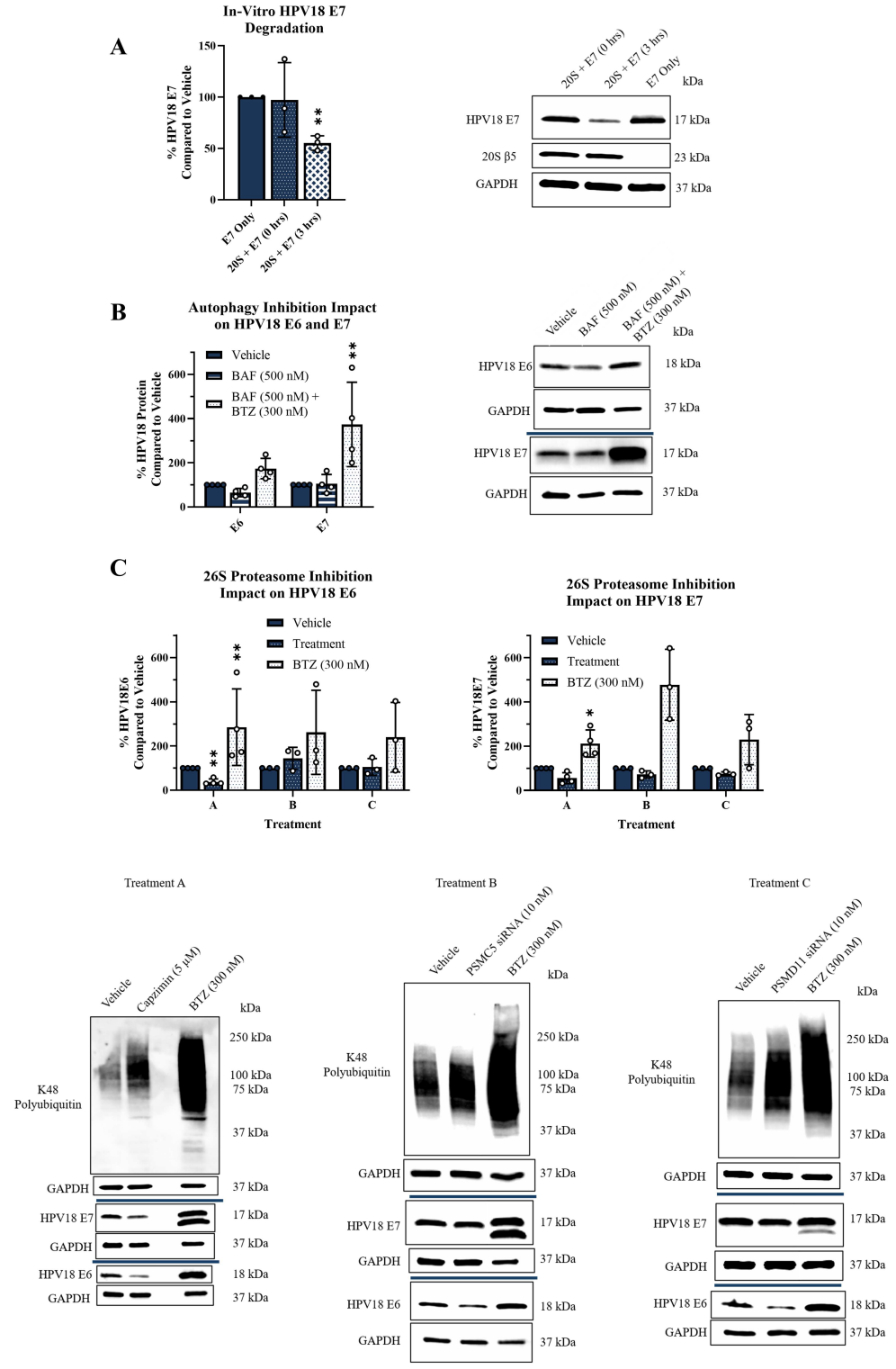


Figure 1

Figure 1

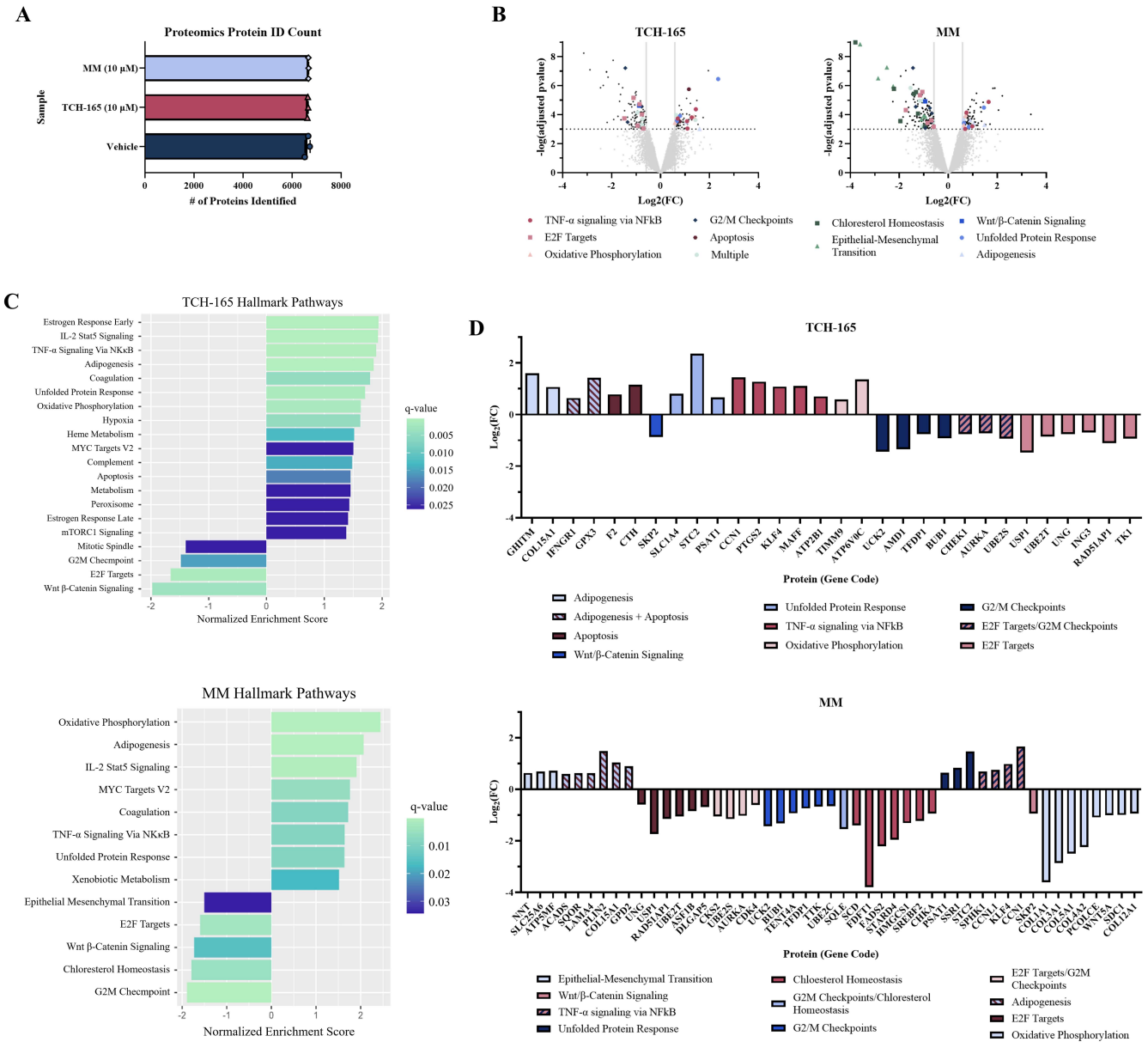


Figure 4

Figure 4

Supplementary Files

This is a list of supplementary files associated with this preprint. Click to download.

- SupplementalInformationOriginalWesternBlots.pdf
- SupplementalInformation2026.pdf